The Interaction between Surfactants and Montmorillonite and its Influence on the Properties of Organo-Montmorillonite in Oil-Based Drilling Fluids

Guanzheng Zhuang, Zepeng Zhang, Shanmao Peng, Jiahua Gao, Francisco Pereira, Maguy Jaber

INTERACTION BETWEEN SURFACTANTS AND MONTMORILLONITE AND ITS INFLUENCE ON THE PROPERTIES OF ORGANO-MONTMORILLONITE IN OIL-BASED DRILLING FLUIDS

Guanzheng Zhuang [1], Zepeng Zhang [1,*], Shanmao Peng [1], Jiahua Gao [1], Francisco A. R. Pereira [2,3], and Maguy Jaber [2,*].

[1] Beijing Key Laboratory of Materials Utilization of Nonmetallic Minerals and Solid Wastes, National Laboratory of Mineral Materials, School of Materials Science and Technology, China University of Geosciences, No. 29, Xueyuan Road, Haidian District, Beijing 100083, PR China

[2] Sorbonne Université, Laboratoire d'Archéologie Moléculaire et Structurale (LAMS), CNRS UMR8220, case courrier 225, UPMC 4 Pl. Jussieu, 75005 PARIS CEDEX 05, France

[3] Chemistry Department, Science and Technology Center, Universidade Estadual da Paraíba, Campina Grande, Paraíba, Brazil.

Corresponding Author:

Zepeng Zhang

Address: School of materials science and technology, China University of Geosciences, Beijing, China.

Tel: +86-010-8232-1845

Fax: +86-10-8232-2974

Email: unite508@163.com

Maguy Jaber

Address: Sorbonne Université, Laboratoire d'Archéologie Moléculaire et Structurale (LAMS), CNRS UMR8220, case courrier 225, UPMC 4 Pl. Jussieu, 75005 PARIS CEDEX 05, France

Tel: +33-(0)1-4427-6289

Fax: +33-(0)1-4427-8298

Email: maguy.jaber@upmc.fr

Received 13 May 2018; revised 6 February 2019; accepted 11 February 2019; Ms 1289

Abstract

The increasing demands of oil and gas and associated difficult drilling operations require oil-based drilling fluids that possess excellent rheological properties and thermal stability. The objective of the present work was to investigate the rheological properties and thermal stability of organo-montmorillonite (OMnt) modified with different surfactants and different loading levels in oil-based drilling fluids, as revealed by the interaction between organic surfactants and montmorillonite. The influence of the structural arrangement of surfactants on the thermal stability of organo-montmorillonite (OMnt) in oil-based drilling fluids was also addressed. OMnt samples were prepared in aqueous solution using surfactants possessing either a single long alkyl chain and or two long alkyl chains. OMnt samples were characterized by X-ray diffraction, high-resolution transmission electron microscopy, thermal analysis, and X-ray photoelectron spectroscopy. Organic surfactants interacted with montmorillonite by electrostatic attraction. The arrangements of organic surfactants depended on the number of long alkyl chains and geometrical shape of organic cations. In addition to the thermal stability of surfactants, intermolecular interaction also improved the thermal stability of OMnt/oil fluids. A tight paraffin-type bilayer arrangement contributed to the excellent rheological properties and thermal stability of OMnt/oil fluids. The deterioration of rheological properties of OMnt/oil fluids at temperatures up to 200°C was due mainly to the release of interlayer surfactants into the oil.

Keywords: Arrangement, Oil-Based Muds, Organo-Clay, Rheological Properties, Thermal Behavior.

INTRODUCTION

Montmorillonite (Mnt) belongs to the general family of phyllosilicates. An ideal Mnt layer is composed of two continuous [SiO_4] tetrahedral sheets (T) and an [AlO_6] octahedral sheet (O). Thus, the structure of Mnt is described as a TOT type (Bergaya *et al.*, 2012). Due to isomorphic substitution, Mnt layers are often negatively charged. A negatively charged layer arises from the substitution of Mg^{2+} and other smaller charge cations for Al^{3+} in octahedral sites (Brigatti *et al.*, 2013; Jaber *et al.*, 2014). Consequently, cations such as Na^{+} and Ca^{2+} present in the interlayer space counterbalance the deficit of positive charges. Significantly, these cations are exchangeable (Lagaly, 1981) with organic cations such as quaternary ammonium salts and quaternary phosphonium salts.

The preparation of organo-montmorillonite (OMnt) with cationic surfactants (Paiva *et al.*, 2008; He *et al.*, 2010; Lagaly *et al.*, 2013), non-ionic surfactants (Shen, 2001; Bertuoli *et al.*, 2014; Guégan *et al.*, 2015), anionic surfactants (Sarier *et al.*, 2010; Zhang *et al.*, 2010), and a mixture of different kinds of surfactants (Chen *et al.*, 2008; Gunawan *et al.*, 2010; Zhang *et al.*, 2013; Wu *et al.*, 2014) is reported commonly. OMnt prepared with cationic surfactants (often quaternary ammonium salts) are used widely in industrial and scientific applications. A substantial industry has been established for years to develop the utilization of OMnt in paint, adsorbents, greases, cosmetics, and nanocomposites, *etc*. (Jaber *et al.*, 2002; Paiva *et al.*, 2008; He

89 *et al.*, 2010; Lee and Tiwari, 2012).

90 An important use of OMnt is as a rheological additive in oil-based drilling fluids
91 (Caenn and Chillingar, 1996; Caenn *et al.*, 2011). Quaternary ammonium salts in
92 which the alkyl chain has 12–22 carbon atoms are usually used to prepare OMnt for
93 oil-based drilling fluids (Dino and Thompson, 2002; Frantz, 2014); for example, cetyl
94 trimethyl ammonium (Zhuang *et al*., 2016; Ratkievicius *et al*., 2017), octadecyl
95 trimethyl ammonium chloride (Zhuang *et al*., 2017a), octadecyl benzyl dimethyl
96 ammonium (Hermoso *et al*., 2014, 2017), and dimethyl dioctadecyl ammonium
97 chloride (Hermoso *et al*., 2014, 2017). With the increasing demands of the oil and gas
98 industry, drilling operations have been undertaken in many difficult wells, such as
99 high-temperature, high-pressure, high-angle, and offshore wells. Oil-based drilling
100 fluids are more popular due to their excellent lubricity, high rate of penetration, shale
101 inhibition, wellbore stability, and good thermal stability (Caenn and Chillingar, 1996;
102 Khodja *et al.*, 2010).

103 Previous studies identified that the rheological properties of oil-based drilling
104 fluids are affected by the concentration and nature of OMnt (Hermoso *et al.*, 2014,
105 2015; Zhuang *et al.*, 2016, 2017a). The lipophilicity of surfactants contributes to the
106 compatibility between oil and OMnt. Furthermore, for the same surfactant, more
107 surfactant usually results in a larger basal spacing and further improves the swelling
108 ability or even exfoliation. Exfoliation of OMnt in oil improves the rheological
109 properties (Zhuang *et al*. 2017a,c). The dissolution of organic surfactants into oil
110 might be a crucial reason for the deterioration of rheological properties at high

111 temperature. Such previous studies mostly reported the relationship between the
112 structure and properties of OMnt and the properties of oil-based drilling fluids.

113 Some problems, however, are still unsettled: (i) how do organic surfactants
114 remain stable on the exfoliated OMnt layers? (ii) what is the reason for the
115 deterioration of rheological properties at high temperatures? and (iii) the influence of
116 the arrangements of interlayer surfactants on the properties of oil-based drilling fluids
117 is unresolved. The purpose of the present study was to try to resolve these problems,
118 using two typical organic surfactants to modify Mnt, by determining the rheological
119 properties and thermal stability of different OMnt samples in oil-based drilling fluids,
120 thus revealing the interaction between organic surfactants and Mnt, and to measure
121 the attendant structural changes in OMnt at the molecular scale.

122

123 MATERIALS AND METHODS

124 *Materials*

125 Mnt was obtained from the Kazuo Shuanglong Mining Co., Ltd, Liaoning
126 Province, China. The mass percentage of montmorillonite included in the Mnt sample
127 was calculated from X-ray diffraction (XRD) patterns (Chinese standard SY/T
128 5163-2010: Analysis method for clay minerals and ordinary non-clay minerals in
129 sedimentary rocks by X-ray diffraction). This method was explained in a previous
130 study (Zhuang *et al.*, 2018). The calculation follows the formula: $X_i = \left[\frac{I_i}{K_i} / \left(\sum \frac{I_i}{K_i}\right)\right] \times$
131 100% , where X_i is the mass percent of phase i; K_i is the intensity ratio of phase i to
132 corundum with the mass ratio i/corundum = 1:1. For the current work, the K values of

minerals are listed in Table 1. The XRD pattern of Mnt (Figure 1) indicated the presence of montmorillonite (88%), quartz (7%), calcite (2%), albite (2%), and pyrite (1%) (Table 2). The cation exchange capacity (CEC) of the Mnt was 120 $cmol_{(+)}$/kg. Cationic surfactant octadecyl trimethyl ammonium chloride (C18) and dimethyl dioctadecyl ammonium chloride (DC18) were purchased from Anhui Super Chemical Technology Co., Ltd, Hefei, Anhui, China. The ideal structures of these two organic cations (Figure 2) were optimized by ChemBio 3D using the molecular mechanics (MM2) minimization program (*Bowen et al.*, 1987). The purity of the surfactants was 99%. The base oil, No. 5 white oil, was obtained from the China National Petroleum Corporation.

Preparation of OMnt

OMnts were prepared in aqueous solution as reported previously (Zhuang *et al.*, 2017a): 100 g of Mnt was added to 1 L of deionized water and stirred for 0.5 h; surfactant was then added to the previous dispersion and the resulting dispersion stirred for 1 h. Finally, after centrifugation, drying at 60°C for 24 h, and milling and sieving with a 200-mesh sieve, OMnt was obtained. C18-modified OMnts were named C18-Mnt-1.0 and C18-Mnt-2.0, where 1.0 and 2.0 indicated that the amounts of C18 were equivalent to 1.0 CEC or 2.0 CEC of Mnt, respectively. Correspondingly, OMnts prepared with DC18 (0.5 CEC and 1.0 CEC of Mnt) were marked as DC18-Mnt-0.5 and DC18-Mnt-1.0.

Preparation of oil-based fluids

Twelve grams of OMnt was added to 400 mL white oil (concentration of 30 kg/m^3) and blended for 20 min at 8000 rpm. A drilling fluid should be aged at different temperatures to model the real drilling operation. The blended fluids were placed in a rotary oven heated to 66°C, 150°C, 180°C, and 200°C in which they were aged for 16 h. All the operations followed the standards of the American Petroleum Institute (API), *i.e.* API SPEC 13A (Specification for Drilling Fluid Materials, 2010) and API RP 13B-2 (Recommended practice for field testing oil-based drilling fluids, 2014). The oil-based fluids were named following the template of OMnt/oil-temperature. For example, C18-Mnt-1.0/oil-66 was prepared by C18-Mnt-1.0 and white oil aged at 66°C.

Characterization

The XRD analysis was conducted using a Bruker D8 Advance X-ray powder diffractometer (Germany), using Cu Kα radiation at 40 kV and 40 mA and a scan speed of 0.05 s per step (step size of 0.02°). The XRD data points covered the range 1.5° to 70°2θ. The transmission electron microscope (TEM) analysis was conducted using Tecnai G2 F20 TEM equipment (Hillsboro, Oregon, USA) and operated under the voltage of 200 kV. Thermogravimetry (TG) analysis was tested on a NETZSCH STA 449 F3 type DTA-TG instrument (Selb, Bavaria, Germany) from room temperature to 900°C in air, with a heating rate of 10°C/min. The X-ray photoelectron spectroscopy (XPS) analysis was carried out using a Thermo escalab 250Xi instrument (Waltham, Massachusetts, USA). Bombardment of the surface with X-rays (monochromated Al Kα radiation, 1486.6 eV) resulted in the emission of

177 photoelectrons with element-specific binding energies (BE). Firstly, a survey scan in
178 the energy range of 1350–0 eV was recorded at a resolution of 1 eV. Then,
179 high-resolution O 1s, Si 2p, Al 2p, C 1s, and N 1s scans were obtained. The
180 rheological properties (apparent viscosity (AV), plastic viscosity (PV), and yield point
181 (YP)) of aged oil-based drilling fluids were determined at 20°C, using a FANN 35A
182 viscometer (Qingdao HaiTongDa Special Purpose Instrument Co., Ltd., China). AV =
183 $1/2\theta_{600}$ (θ_{600} is the dial reading at 600 rpm, corresponding to a shear rate of 1021.8 s^{-1}).
184 PV = θ_{600}–θ_{300} and YP = $1/2(\theta_{300}$–PV). The dynamic rheological behavior of oil-based
185 fluids was measured using a Themo Scientific HAAKE Roto Visco 1 rotational
186 viscometer (USA). The programmed measurement regime was: the shear rate
187 increased linearly from 0 s^{-1} to 100 s^{-1} in 5 min (up step), and then decreased linearly
188 from 100 s^{-1} to 0 s^{-1} in 5 min (down step).
189
190 RESULTS AND DISCUSSION
191 *XRD of OMnt powders*
192 The basal reflection of Mnt occurred at 7.05°2θ, corresponding to d_{001} = 1.25 nm
193 (Figure 1). After organic modification, the basal spacing of OMnt increased (Figure 3),
194 giving d_{001} values for C18-Mnt-1.0, C18-Mnt-2.0, DC18-Mnt-0.5, and DC18-Mnt-1.0
195 of 2.12 nm, 4.06 nm, 3.51 nm, and 3.68 nm, respectively. The d_{001} of C18-Mnt-2.0 is
196 almost double the d_{001} of C18-Mnt-1.0. In the case of DC18-modified OMnt, however,
197 the d_{001} of DC18-Mnt-1.0 increased by ~5% over DC18-Mnt-0.5. This phenomenon
198 indicated that C18 and DC18 occupied very different structural arrangements in OMnt.

The (002) and (003) reflections emerged in the XRD patterns of C18-Mnt-2.0, DC18-Mnt-0.5, and DC18-Mnt-1.0, whereas no peaks can be referred to (002) and (003) reflections in the XRD pattern of C18-Mnt-1.0. The basal reflection intensity showed the sequence of DC18-Mnt-1.0 > C18-Mnt-2.0 > DC18-Mnt-0.5 > C18-Mnt-1.0. Thus, the order of the degree of layer stacking (along the *c* axis) follows DC18-Mnt-1.0 > C18-Mnt-2.0 > DC18-Mnt-0.5 > C18-Mnt-1.0. DC18 likely was arranged in a more ordered manner in the interlayer space than C18.

TEM analysis

High-resolution TEM images (Figure 4) gave information about the basal spacing and the thickness of platelets. The TEM images of raw Mnt showed tightly stacked aluminosilicate layers. The thickness of the platelets of raw Mnt was >50 nm and the lamellae contained >50 layers. The lamellae of OMnt were thicker than those of raw Mnt and contained fewer layers. For both C18- and DC18-modified OMnt, more surfactant led to thicker lamellae. The thickness of C18-Mnt-1.0 lamellae was a little larger than that of DC18-Mnt-0.5 lamellae, and the thicknesses of C18-Mnt-2.0 and DC18-Mnt-1.0 lamellae were similar. This fact indicates that 1.0 CEC DC18 and 2.0 CEC C18 resulted in similar effects on the thickness of OMnt lamellae.

The TEM images also revealed the basal spacing directly. The layers in C18-Mnt-1.0 were not arranged neatly and the basal spacing ranged from 1.44 to 1.79 nm. Ordered stacking of layers was observed in the TEM images of C18-Mnt-2.0, DC18-Mnt-0.5, and DC18-Mnt-1.0. DC18-modified OMnt samples were more likely

to exhibit an ordered arrangement of layers. More surfactant also led to ordered layer stacking. The basal spacing derived from the TEM images, however, was smaller than the results derived from XRD (Table 3). This phenomenon might be caused by the radiation damage from the high voltage (200 kV). The lattices of clay minerals are easily damaged by high voltage in high-resolution TEM (Kogure, 2013). Surfactants would degrade under high voltage, resulting in the decrease of basal spacing. Δd_{001} indicated the change of arrangement of the interlayer surfactants. C18-Mnt-2.0 exhibited the largest Δd_{001} value, demonstrating the dramatic re-organization of interlayer surfactants under high voltage. The similar Δd_{001} values of DC18-Mnt-0.5 and DC18-Mnt-1.0 suggested similar arrangements of interlayer surfactants in these two OMnt samples.

Thermal analysis

Mnt showed two steps of mass loss (Figure 5). The first step (<150°C), corresponding to a mass loss of 6.8%, was attributed to the loss of the water molecules on the surface and in the interlayer space of Mnt (He *et al.*, 2005; Zhuang *et al.*, 2015). The second mass loss step (500–745°C, mass loss of 6.3%) represented the dehydration of hydroxyl groups coordinated by the structural cations in tetrahedral and octahedral sites (Greene-Kelly, 1957; Hedley *et al.*, 2007). The organic surfactants completely decompose above 500°C. The onset temperatures (T_{onset}) corresponding to the thermal decomposition of C18 and DC18 were 202°C and 145°C, respectively, indicating that C18 is more thermally stable than DC18.

In summary, dehydration of adsorbed water (below 150°C), oxidation of organic surfactants (150°C to 430°C), continuous oxidation of organic surfactants (430°C to 650°C), and dehydration of hydroxyl groups (650°C to 800°C) can be observed in the TG and DTG curves of OMnt. The percentage water loss from C18-Mnt-1.0, C18-Mnt-2.0, DC18-Mnt-0.5, and DC18-Mnt-1.0 was 2.2%, 1.8%, 0.8%, and 0.0%, respectively. OMnt samples contained less water than Mnt. In addition, C18-modified OMnt samples contained more adsorbed water than DC18-modified OMnt samples. The main factors affecting the interlayer hydration of montmorillonite include: (i) hydration energy of the interlayer cations, (ii) polarization of the water molecules by interlayer cations, (iii) variation of the electrostatic surface potentials because of differences in layer charge locations, (iv) activity of water, and (v) size and morphology of the clay particles (Brigatti *et al.*, 2013). Although C18 and DC18 cations had the same positive charges with Na^+ cations, the organic cations showed a larger size and lower polarity due to the alkyl chains. In addition, the hydrophobicity of organic cations could prevent the adsorption of water. DC18 cations exhibited a larger size and better hydrophobicity than C18 cations, resulting in less interlayer water in the DC18-modified OMnt.

The T_{onset} corresponding to the thermal decomposition of organic surfactants in OMnt samples revealed the thermal stability of the samples. The T_{onset} values of C18, C18-Mnt-1.0, and C18-Mnt-2.0 were 202°C, 185°C, and 175°C, respectively. The T_{onset} values of DC18, DC18-Mnt-0.5, and DC18-Mnt-1.0 were 145°C, 180°C, and 159°C, respectively. C18-modified OMnt, therefore, showed better thermal stability

than DC18-modified OMnt. For C18-modified OMnt, the T_{onset} value was lower than that of C18 because organic surfactants not only intercalated into the interlayer space, but also occupied the outer surface (He *et al.*, 2005; Hedley *et al.*, 2007; Zhu *et al.*, 2011). The interlayer surfactants were protected by the Mnt layers. However, the surfactants exposed on the external surface were more susceptible to thermal degradation without the protection of the Mnt interlayers. Evidently, surfactants were mostly intercalated in the interlayer space when the surfactant loading level was <1.0 CEC of Mnt. When more surfactant was used, more should have adsorbed on the external surface, resulting in the decrease of T_{onset} (Zhuang *et al.*, 2016). For DC18-modified OMnt, most of the surfactant was intercalated into the interlayer space due to the smaller amount of surfactant (≤1.0 CEC). Accordingly, DC18-Mnt exhibited better thermal stability than the pure surfactant.

XPS analysis

The XPS survey scans of Mnt (Figure 6) showed the presence of O, Si, Al, Mg, Fe, Na, and C in Mnt. The presence of C in Mnt was assigned to calcite. After surfactant modification, the signals of N and Cl emerged in the spectra of OMnt samples. In addition, the intensity of the C 1s signal in OMnt was much greater than that in Mnt, demonstrating the adsorption and intercalation of organic surfactants. The signals of Cl 2s and Cl 2p in C18-Mnt-2.0 were more intense than those in other OMnt samples. This phenomenon indicated that more Cl^- ions are included in C18-Mnt-2.0, because the excess surfactant (more than 1.0 CEC of Mnt) cannot

intercalate into the interlayer space *via* cation exchange but remains neutral as an ion pair with Cl^- (He *et al.*, 2007).

Oxygen is the element most exposed on the surface of Mnt and TOT layers. Interaction between Mnt and surfactants should, therefore, first affect the binding energy of O. The binding energy of O 1s in Mnt was 532.5 eV (Figure 7), representing oxygen in Si-O(H) and Al(Mg, Fe)-O(H) groups. Compared with Mnt, the binding energy of O 1s in OMnt samples was smaller, indicating greater electron density around O atoms in OMnt. The high-resolution XPS scans of Si 2p (Figure 8) and Al 2p (Figure 9) also showed a decrease in binding energy, suggesting that the $[SiO_4]$ tetrahedra and $[Al(Mg, Fe)O_6]$ octahedra, as a whole, exhibited higher electron densities after organic modification.

The C 1s spectra (Figure 10) of surfactants can be distinguished as two parts: C-C groups corresponding to a binding energy of 284.8 eV and C-N groups corresponding to 285.9 eV (C18) and 286.0 eV (DC18) (He *et al.*, 2007; Schampera *et al.*, 2015). The binding energy of C 1s involving C-C groups maintained a constant value of 284.8 eV after organic modification, indicating no interaction involving the long alkyl chains. The binding energy of C 1s spectra involving C-N groups, however, shifted to larger values, demonstrating the decline of electron density around C atoms connecting with N. From the high-resolution XPS spectra of N 1s (Figure 11) in organic surfactants, the binding energy of N 1s was 402.1 eV. However, the binding energy of N 1s in OMnt increased slightly, demonstrating a decrease of electron density around N. The decrease of binding energies of N 1s and C 1s in the C-N

groups proved that the reduction of electron density occurs only in the polar heads of surfactants, without the long alkyl chains.

From the high-resolution XPS spectra, the interaction between Mnt and organic surfactants occurred between the TOT layers of Mnt and polar heads of surfactants. TOT layers were electron acceptors and the polar heads of organic surfactants were electron donors. The shift of the binding energy (ΔBE) (Table 4) value of O 1s was in the range of –1.2 to –1.0 eV. The ΔBE value of C 1s (C-N) was between 0.3 and 0.5 eV and that of N 1s was in the range 0.1–0.3 eV. Two conclusions can be drawn from the XPS results: (i) no new signals emerged in the XPS spectra, except for small changes in binding energy; (ii) compared with Mnt and surfactants, the binding energy of Mnt elements (O 1s, Si 2p and Al 2p) in OMnt decreased while the surfactant elements (C 1s and N 1s) in OMnt increased. Considering the negatively charged Mnt layers and organic cations, the XPS results demonstrate electrostatic attraction between the TOT layers and the polar heads of surfactants, without chemical bonds. The binding energy of O 1s in C18-Mnt-2.0 showed the smallest shift because extra surfactants intercalate into the interlayer space in the form of ion pairs (Cl^- anions and C18 cations). DC18-modified OMnt samples showed smaller ΔBE values than C18-modified OMnt samples, due to the conjugated effect of two long alkyl chains.

Arrangements and interactions of interlayer surfactants

Electrostatic attraction between Mnt and the polar heads of surfactants is affected

only by the quantity of electricity. Thus, electrostatic attraction is irrelevant to the molecular size or conformation. Previous reports revealed that OMnt modified with different surfactants exhibited different properties and thermal stability. Hence, the interaction between organic surfactants should be considered. C18 cations, having a single long alkyl chain, can be considered as having a 'linear shape' and DC18 cations can be regarded as being 'V-shaped' due to its two long alkyl chains (Figure 1). Interlayer surfactants arrange themselves as lateral-monolayer, lateral-bilayer, pseudo-trimolecular layer, paraffin-type monolayer. or paraffin-type bilayer (Vaia *et al.*, 1994; Lagaly *et al.*, 2013). The arrangements of interlayer surfactants are influenced by the loading level, conformation of surfactants, the length of the alkyl chain, and even the charge of Mnt. Short-chain alkylammonium cations are arranged in monolayers and longer chain alkylammonium ions in bilayers with the alkyl chain axes parallel to the silicate layers (Lagaly *et al*., 2013); a pseudo-trimolecular arrangement is often observed with highly charged smectites and/or long surfactant cations. The periodicity along the *c* axis of Mnt (without cations and water) is 0.96 nm (Brigatti *et al*., 2013). Considering the size of the C18 cation (Figure 1), C18-modified OMnts ideally exhibit a basal spacing of 1.33 nm with a monolayer arrangement, 1.73 nm with a bilayer arrangement, and 2.19 nm with a pseudo-trimolecular arrangement. Lagaly *et al*. (2013) concluded that the monolayer arrangement had a basal spacing of 1.4 nm, the bilayer 1.8 nm, and the pseudo-trimolecular arrangement 2.2 nm. Thus, the basal spacing (2.12 nm) of C18-Mnt-1.0 suggests that C18 molecules were arranged as a pseudo-trimolecular

353 layer (Figure 12). The positive heads of C18 were attached on the silicate layers,
354 whereas the alkyl chains assumed a trimolecular arrangement by the formation of
355 kinks. The pseudo-trimolecular arrangement of C18 cannot result in ordered
356 arrangements of C18 cations in the interlayer space. In addition, the octadecyl chains
357 could kink by formation of gauche bonds at different C atoms (Lagaly, 1976). Hence,
358 the arrangement of C18 molecules was not sufficiently homogeneous to form very
359 ordered stacks of layers. Only the low-intensity (001) reflection, therefore, emerged in
360 the XRD patterns of C18-Mnt-1.0; the TEM image also testified to the non-uniform
361 basal spacing. With the increase of loading level or alkyl chain length, organic cations
362 tended to be arranged as a paraffin-type in a tilted to vertical arrangement (Lagaly,
363 1986). Based on the basal spacing of 4.06 nm, C18-Mnt-2.0 nm is proposed to be
364 arranged as a tilted paraffin-type bilayer (Figure 12). The tilting angle, θ, is correlated
365 positively with the amount of intercalated organic surfactants. In the case of
366 C18-Mnt-2.0, θ is 52°. 1.0 CEC organic cations were assumed to exchange all the
367 inorganic cations and occupy all the negative sites. The extra 1.0 CEC surfactants
368 cannot intercalate into the interlayers completely because all of the exchangeable sites
369 had been occupied. They should be adsorbed in the form of ion pairs (with anions).
370 More surfactant molecules resulted in a tight arrangement, which made every single
371 surfactant molecule hard to move. Consequently, C18-Mnt-2.0 showed a more
372 ordered structure and displayed (002) and (003) reflections.

373 Quaternary alkylammonium ions with two or more long alkyl chains often form
374 paraffin-type arrangements in the interlayer space of smectites (Lagaly *et al.*, 2013).

DC18 has two long octadecyl chains. Considering the size of the DC18 and the basal spacing of OMnt, DC18 molecules in the interlayer space of DC18-Mnt-0.5 and DC18-Mnt-1.0 must arrange themselves in the form of a paraffin-type bilayer (Figure 12). The angle between the two octadecyl chains varied with the loading level. The most stable conformation of DC18 corresponded to an angle of ~118.9°. This angle, however, must gradually reduce in order to accommodate more DC18 cations, *i.e.* $\alpha > \varphi > \gamma$. Finally, an almost parallel orientation of the chains was attained by formation of gauche bonds near the ammonium group. The conformation of DC18 cations allowed a denser packing of these surfactants in mono-and bimolecular films (Favre and Lagaly, 1991). This intensive arrangement with a strong interaction between DC18 cations bound individual cations together.

Rheological properties of OMnt in oil

Drilling fluids are often evaluated using the Bingham plastic flow model and are often required to work in high-temperature conditions with low viscosity. Generally, AV is used as the effective viscosity to evaluate the viscosity of drilling fluids. PV is not expected to be too high, because extremely high PV would make starting to drill difficult. The rheological properties of OMnt/oil drilling fluids (AV, PV, and YP) vary with different temperatures of ageing (Table 5). A commercial OMnt (DG-Mnt), as used by Mud Service Company, Bohai Drilling Engineering Co. Ltd, was used as a reference. DG-Mnt/oil, C18-Mnt-1.0/oil, and DC18-Mnt-0.5/oil fluids all showed quite low viscosities and yield points. Their yield points were zero or very close to

zero, indicating these OMnt/oil fluids possessed no gel strength. Although the values of AV, PV, and YP were stable, the thermal stabilities of DG-Mnt/oil, C18-Mnt-1.0/oil, and DC18-Mnt-0.5/oil fluids were meaningless because of their poor rheological properties. Compared to the rheological properties of DG-Mnt/oil, C18-Mnt-1.0/oil, and DC18-Mnt-0.5/oil fluids, the rheological properties of C18-Mnt-2.0/oil and DC18-Mnt-1.0/oil fluids were dramatically increased. This result demonstrates that more surfactants lead to better rheological properties. C18-Mnt-2.0 showed bigger d_{001} than DC18-Mnt-1.0; however, DC18-Mnt-1.0/oil fluids presented better rheological properties than C18-Mnt-2.0/oil fluids. This phenomenon testifies that a bigger basal spacing does not necessarily result in better rheological properties. The rheological properties of OMnt in oil-based drilling fluids should not be influenced only by surfactant loading level and basal spacing, but also by the arrangements of interlayer surfactants. The AV and YP of both C18-Mnt-2.0/oil and DC18-Mnt-1.0/oil fluids firstly increased and finally decreased with rising temperature. For example, the viscosity of C18-Mnt-2.0/oil fluid increased from 16.5 mPa s at 66°C to 31.0 mPa·s at 150°C, then decreased to 26.5 mPa s at 180°C and 24.0 mPa s at 200°C. The AV of DC18-Mnt-1.0/oil fluid and the YP of C18-Mnt-2.0/oil and DC18-Mnt-1.0/oil fluids are affected similarly. Viscosity and gel strength improved with increasing temperature because higher temperatures promote the swelling and even exfoliation of OMnt in oil (Zhuang *et al.*, 2017a, 2017c). Temperature increase above 180°C, however, was harmful for rheological properties. Focusing on the rheological properties of OMnt/oil fluids aged at 150 to 200°C, DC18-Mnt-1.0/oil fluid was more

stable than C18-Mnt-2.0/oil fluid. The AV of DC18-Mnt-1.0/oil fluid decreased from 47.0 mPa s to 40.0 mPa s and the YP decreased from 18.0 Pa to 15.0 Pa. But the AV of C18-Mnt-2.0/oil fluid decreased from 31.0 mPa s to 24.0 mPa s and the YP decreased from 15.0 Pa to 3.0 Pa.

The dynamic rheological curves of OMnt/oil fluids (Figure 13) revealed rheological behavior and thixotropy. The DG-Mnt/oil, C18-Mnt-1.0/oil, and DC18-Mnt-0.5/oil fluids showed non-linear curves and presented low shear stress, in agreement with the results in Table 5. The rheological curves of DG-Mnt/oil, C18-Mnt-1.0/oil, and DC18-Mnt-0.5/oil can be divided into two parts: (i) the Bingham plastic model (a line which does not cross the zero point) in the range of 20–100 s^{-1}; (ii) deviation from the Bingham plastic model to the zero point. DC18-Mnt-1.0/oil fluid exhibited greater shear stress than C18-Mnt-2.0/oil fluid. The shear stress of C18-Mnt-2.0/oil decreased dramatically from 150°C to 200°C. However, the rheological curve of DC18-Mnt-1.0/oil aged at 180°C nearly coincided with that of DC18-Mnt-1.0/oil aged at 150°C. When the temperature increased to 200°C, the shear stress decreased a little.

Thixotropy is another important rheological property. It is a reversible isothermal transformation of a colloidal sol to a gel. In drilling practice, low resistance (low viscosity) is expected for the bit to ensure a rapid drilling rate, while high viscosity is needed for carrying cuttings. Excellent thixotropy is, thus, a necessary property of an oil-based drilling fluid. The areas of thixotropic loops (Figure 13) were applied to evaluate thixotropy of OMnt/oil fluids. The areas were calculated by integration

441 (Table 6). Similarly with the viscosity results, DG-Mnt/oil, C18-Mnt-1.0/oil, and
442 DC18-Mnt-0.5/oil fluids showed very small areas, indicating nearly no thixotropy of
443 these fluids. The area of C18-Mnt-2.0/oil aged at 66°C is 2.61 Pa s^{-1}. It increased to
444 193.43 Pa s^{-1} at 150°C, then decreased to 27.50 Pa s^{-1} at 200°C, declining by 86%
445 from the area at 150°C. The area of DC18-Mnt-1.0/oil aged at 66°C was 26.21 Pa s^{-1}
446 and then increased to 424.68 Pa s^{-1}, indicating that high temperature below 150°C
447 promotes thixotropy. With the temperature rising to 200°C, the area decreased to
448 324.85 Pa s^{-1} at 200°C, down by 19% from that at 150°C. This result demonstrated
449 that the thixotropy of DC18-Mnt-1.0/oil fluid was more stable than that of
450 C18-Mnt-2.0/oil fluid.

451 In conclusion, the rheological properties and thermal stability followed the order
452 of DC18-Mnt-1.0/oil > C18-Mnt-2.0/oil > DC18-Mnt-0.5/oil ≈ C18-Mnt-2.0/oil. Two
453 possible reasons for decrease of rheological properties at high temperatures can be
454 proposed: (i) thermal decomposition of surfactants and (ii) dissolution of interlayer
455 surfactants into oil. Based on the thermal analysis results, DC18-Mnt-1.0 started to
456 decompose below 180°C (in air). But DC18-Mnt-1.0/oil fluid showed very stable
457 rheological properties at 200°C, indicating the thermal stability of OMnt in oil was
458 improved due to the lack of oxygen. Thus, the decline of other OMnt/oil fluids below
459 200°C was not caused by thermal decomposition. The only possibility is the
460 dissolution of interlayer surfactants into oil at high temperature. The HLB values of
461 C18 and DC18 are 14.9 and 6.8. DC18 showed more lipophilicity than C18.
462 DC18-Mnt-1.0, however, led to more stable rheological properties than C18-Mnt-2.0,

463 indicating that the paraffin-type bilayer of DC18 in OMnt can resist high temperatures
464 better than the paraffin-type bilayer of C18.
465
466 *XRD of OMnt/oil gels*
467 To reveal the relationship between the thermal stability of OMnt/oil fluids and
468 the arrangement of surfactants in the interlayer space of OMnt, the structure of OMnt
469 in oil must be known. The structural change of OMnt in oil can be determined by
470 XRD of OMnt/oil gel (Figure 14). All the samples showed a wide and low-intensity
471 reflection at 17°2θ, which is assigned to the oil (Zhuang *et al.*, 2017b). Two
472 reflections, corresponding to *d* values of 2.05–2.06 nm and 1.38–1.43 nm, emerged in
473 the C18-Mnt-1.0/oil aged at 66°C, 150°C, and 180°C. The *d* values of these two
474 reflections were smaller than the basal spacing of C18-Mnt-1.0 (2.12 nm), suggesting
475 that the d_{001} of C18-Mnt-1.0 in oil was reduced. Thermal analysis results proved that
476 C18-Mnt-1.0 was stable up to 180°C. Therefore, the decrease of basal spacing must
477 be due to the surfactants dissolving in oil. These two reflections cannot be attributed
478 to (001) and (002) reflections, because the *d* value of the second reflection is not half
479 that of the first. The two reflections, therefore, represented different basal spacings,
480 indicating that the interlayer surfactants dissolved into oil gradually. The surfactants
481 on the surfaces and edges dissolved first, then the internal surfactants dissolved,
482 resulting in two reflections. Finally, aged at 200°C, most of the surfactants in the
483 interlayer space were lost, leading to one reflection with *d* value of 1.36 nm. This
484 phenomenon also demonstrated that high temperature promoted the dissolution of

interlayer surfactants, possibly because high temperature facilitated the thermal motion of oil molecules and surfactant molecules. A similar phenomenon happened to DC18-Mnt-0.5/oil fluid. The shrinkage of basal spacings of C18-Mnt-1.0 and DC18-Mnt-0.5 in oil demonstrated that loose arrangements resulted in the easy loss of interlayer surfactants. The basal spacing of C18-Mnt-2.0 increased gradually as the temperature increased to 180°C. The basal spacing of C18-Mnt-2.0 in oil reached a maximum value of 4.33 nm when aged at 150°C, corresponding to the best rheological properties of C18-Mnt-2.0/oil fluid. Aged at 200°C, the basal spacing of C18-Mnt-2.0 in oil declined to 1.39 nm. Although C18 cations and molecules are arranged tightly, the interlayer C18 was still lost at high temperature because no strong interaction force exists among the surfactants.

DC18-Mnt-1.0/oil-66 showed a similar reflection to DC18-Mnt-1.0 powder, indicating that no swelling happened, and no surfactants were lost. Because of the tight arrangement of DC18 in OMnt, no extra space was available to accept oil molecules. Below 15°2θ, no reflection is observed in the XRD patterns of DC18-Mnt/oil gels aged at high temperatures, while the (100) reflection remained. Thus, DC18-Mnt-1.0 was exfoliated in oil at high temperatures because of thermal motion and interaction among surfactants. Surfactants in the interlayer space were protected by silicate layers, resulting in stabilization. DC18 cations could still remain stably on the surface of exfoliated layers because the strong interaction between DC18 cations fixed them tightly on the nanolayers. Hence, tight arrangement and strong interaction are necessary for the stability of OMnt in oil based-drilling

fluids.

CONCLUSION

Based on the results and discussions above, several conclusions can be drawn. Organic surfactants occupy the surface and interlayer space of Mnt by electrostatic attraction. Interaction happens between the Mnt layers and polar heads of surfactants only. Interaction between organic cations has a critical influence on the stability of OMnt in oil. The style of arrangement of a surfactant with a single long alkyl chain changed from a pseudo-trimolecular layer to a paraffin-tape bilayer with the increase of the surfactant's loading level. Surfactants with two long alkyl chains arranged as a paraffin-type. Paraffin-type arrangements were more ordered than pseudo-trimolecular layers. A paraffin-type bilayer arrangement of DC18 resulted in more ordered layer stacking than the same arrangement of C18. Tight paraffin-type bilayer arrangements generally led to excellent rheological properties and thermal stability. Loose paraffin-type, pseudo-trimolecular layer and tilted bilayer arrangements resulted in easy dissolution of interlayer organic cations into oil at high temperature. A tight paraffin-type bilayer arrangement of DC18 led to exfoliation of OMnt in oil at high temperatures, improving rheological properties. Organic cations can remain stable in the interlayer space or even on the exfoliated Mnt layers because of the strong interaction force among cations, in addition to the electrostatic attraction. In conclusion, to improve the rheological properties and thermal stability of OMnt in oil-based drilling fluids, more than 1.0 CEC surfactants with two or three long alkyl

chains are advised.

Acknowledgments

This work was supported financially by the Fundamental Research Funds for Central Universities (China). The support provided by the China Scholarship Council (CSC) during the visit of Guanzheng Zhuang (No. 201706400010) to Sorbonne Université is acknowledged.

REFERENCES

Bergaya, F., Jaber, M., and Lambert, J.F. (2012) *Clays and clay minerals as layered nanofillers for (bio)polymers*. Pp. 41-75. Springer London.

Bertuoli, P.T., Piazza, D., Scienza, L.C., and Zattera, A.J. (2014) Preparation and characterization of montmorillonite modified with 3-aminopropyltriethoxysilane. *Applied Clay Science*, **87**, 46-51.

Bowen, J. P., Pathiaseril, A., Profeta Jr, S., and Allinger, N. L. (1987) New molecular mechanics (MM2) parameters for ketones and aldehydes. *The Journal of Organic Chemistry*, **52**(23), 5162-5166.

Brigatti, M.F., Galan, E., and Theng, B.K.G. (2013) Chapter 2 structures and mineralogy of clay minerals. Pp. 21-81. In F. Bergaya, and G. Lagaly, Eds. *Developments in clay science*, 5,Elsvier, Netherland.

Caenn, R. and Chillingar, G.V. (1996) Drilling fluids: State of the art. *Journal of Petroleum Science and Engineering*, **14**, 221-230.

551 Caenn, R., Darley, H.C., and Gray, G.R. (2011) *Composition and properties of drilling*
552 *and completion fluids*. Gulf professional publishing, Houston.
553 Chen, D., Zhu, J.X., Yuan, P., and Yang, S.J. (2008) Preparation and characterization of
554 anion-cation surfactants modified montmorillonite. *Journal of Thermal*
555 *Analysis and Calorimetry*, **94**, 841-848.
556
557 Dino, D. and Thompson, J. (2002). U.S. Patent No. 6,462,096. Washington, DC: U.S.
558 Patent and Trademark Office.
559 Favre, H. and Lagaly, G. (1991) Organo-bentonites with quaternary alkylammonium
560 ions. *Clay Minerals*, **26**, 19-32.
561 Frantz, E. B. (2014). U.S. Patent No. 0,011,712. Washington, DC: U.S. Patent and
562 Trademark Office.
563 Greene-Kelly R. (1957) The montmorillonite minerals. In: Mackenzie RC, Editor. *The*
564 *differential thermal investigation of clays*. London: Mineral Society, p 140-164.
565 Guégan, R., Giovanela, M., Warmont, F., and Motelica-Heino, M. (2015) Nonionic
566 organoclay: A 'swiss army knife' for the adsorption of organic micro-pollutants?
567 *Journal of Colloid and Interface Science*, **437**, 71-79.
568 Gunawan, N.S., Indraswati, N., Ju, Y.H., Soetaredjo, F.E., Ayucitra, A., and Ismadji, S.
569 (2010) Bentonites modified with anionic and cationic surfactants for bleaching
570 of crude palm oil. *Applied Clay Science*, **47**, 462-464.
571 He, H., Ding, Z., Zhu, J., Yuan, P., Xi, Y., Yang, D., and Frost, R.L. (2005) Thermal
572 characterization of surfactant-modified montmorillonites. *Clays and Clay*

573 *Minerals*, **53**, s319.
574 He, H., Ma, Y., Zhu, J., Yuan, P., and Qing, Y. (2010) Organoclays prepared from
575 montmorillonites with different cation exchange capacity and surfactant
576 configuration. *Applied Clay Science*, **48**, 67-72.
577 He, H., Zhou, Q., Frost, R.L., Wood, B.J., Duong, L.V., and Kloprogge, J.T. (2007) A
578 x-ray photoelectron spectroscopy study of hdtmab distribution within
579 organoclays. *Spectrochimica Acta Part A Molecular and Biomolecular*
580 *Spectroscopy*, **66**, 1180-1188.
581 Hedley, C.B., Yuan, G., and Theng, B.K.G. (2007) Thermal analysis of
582 montmorillonites modified with quaternary phosphonium and ammonium
583 surfactants. *Applied Clay Science*, **35**, 180-188.
584 Hermoso, J., Martinez-Boza, F., and Gallegos, C. (2014) Influence of viscosity
585 modifier nature and concentration on the viscous flow behavior of oil-based
586 drilling fluids at high pressure. *Applied Clay Science*, **87**, 14-21.
587 Hermoso, J., Martinez-Boza, F., and Gallegos, C. (2015) Influence of aqueous phase
588 volume fraction, organoclay concentration and pressure on invert-emulsion oil
589 muds rheology. *Journal of Industrial and Engineering Chemistry*, **22**, 341-349.
590 Hermoso, J., Martínez-Boza, F. J., and Gallegos, C. (2017). Organoclay influence on
591 high pressure-high temperature volumetric properties of oil-based drilling
592 fluids. *Journal of Petroleum Science and Engineering*, **151**, 13-23.
593 Jaber, M., Georgelin, T., Bazzi, H., Costatorro, F., and Clodic, G. (2014) Selectivities in
594 adsorption and peptidic condensation in the (arginine and glutamic

595 acid)/montmorillonite clay system. *Journal of Physical Chemistry C*, **118**,
596 25447-25455.
597 Jaber, M., Miehe-Brendle, J., and Dred, R.L. (2002) Mercaptopropyl al-mg
598 phyllosilicate: Synthesis and characterization by xrd, ir, and nmr. *Chemistry*
599 *Letters*, **80**, 954-955.
600 Khodja, M., Canselier, J.P., Bergaya, F., Fourar, K., Khodja, M., Cohaut, N., and
601 Benmounah, A. (2010) Shale problems and water-based drilling fluid
602 optimisation in the hassi messaoud algerian oil field. *Applied Clay Science*, **49**,
603 383-393.
604 Kogure, T. (2013) Chapter 2.9 - electron microscopy. Pp. 275-317. In F. Bergaya, and G.
605 Lagaly, Eds. *Developments in clay scinence*, 5,Elsevier, Netherlands.
606 Lagaly, G. (1976) Kink-block and gauche-block structures of bimolecular films.
607 *Angewandte Chemie International Edition*, **15**, 575-586.
608 Lagaly, G. (1981) Characterization of clays by organic compounds. *Clay minerals*,
609 **16**(1), 1-21.
610 Lagaly, G. (1986) Interaction of alkylamines with different types of layered compounds.
611 *Solid State Ionics*, **22**, 43-51.
612 Lagaly, G., Ogawa, M., and Dékány, I. (2013) Chapter 10.3 clay mineral–organic
613 interactions. Pp. 435-505. In F. Bergaya, G.B.K. Theng, and G. Lagaly, Eds.
614 *Developments in clay science*, 5,Elsevier.
615 Lee, S.M. and Tiwari, D. (2012) Organo and inorgano-organo-modified clays in the
616 remediation of aqueous solutions: An overview. *Applied Clay Science*, **s 59–60**,

84–102.

Paiva, L.B.D., Morales, A.R., and Díaz, F.R.V. (2008) Organoclays: Properties, preparation and applications. *Applied Clay Science*, **42**, 8-24.

Ratkievicius, L. A., Da Cunha Filho, F. J. V., Neto, E. L. D. B., Santanna, V. C. (2017). Modification of bentonite clay by a cationic surfactant to be used as a viscosity enhancer in vegetable-oil-based drilling fluid. *Applied Clay Science*, **135**, 307-312.

Sarier, N., Onder, E., and Ersoy, S. (2010) The modification of na-montmorillonite by salts of fatty acids: An easy intercalation process. *Colloids and Surfaces A Physicochemical and Engineering Aspects*, **371**, 40-49.

Schampera, Solc, B., Woche, R., Mikutta, S.K., Dultz, R., Guggenberger, S., Tunega, G., and D. (2015) Surface structure of organoclays as examined by x-ray photoelectron spectroscopy and molecular dynamics simulations. *Clay Minerals*, **50**, 353-367.

Shen, Y. H. (2001) Preparations of organobentonite using nonionic surfactants. *Chemosphere*, **44**, 989-995.

Vaia, R.A., Teukolsky, R. K., and Giannelis, E.P. (1994) Interlayer structure and molecular environment of alkylammonium layered silicates. *Chemistry of Materials*, **6**, 1017-1022.

Wu, S., Zhang, Z., Wang, Y., Liao, L., and Zhang, J. (2014) Influence of montmorillonites exchange capacity on the basal spacing of cation–anion organo-montmorillonites. *Materials Research Bulletin*, **59**, 59–64.

639 Zhang, Z., Liao, L., and Xia, Z. (2010) Ultrasound-assisted preparation and
640 characterization of anionic surfactant modified montmorillonites. *Applied Clay*
641 *Science*, **50**, 576-581.
642 Zhang, Z., Zhang, J., Liao, L., and Xia, Z. (2013) Synergistic effect of cationic and
643 anionic surfactants for the modification of ca-montmorillonite. *Materials*
644 *Research Bulletin*, **48**, 1811-1816.
645 Zhu, J., Qing, Y., Wang, T., Zhu, R., Wei, J., Tao, Q., Yuan, P., and He, H. (2011)
646 Preparation and characterization of zwitterionic surfactant-modified
647 montmorillonites. *Journal of Colloid and Interface Science*, **360**, 386-392.
648 Zhuang, G., Gao, J., Chen, H., and Zhang, Z. (2018) A new one-step method for
649 physical purification and organic modification of sepiolite. *Applied Clay*
650 *Science*, **153**, 1-8.
651 Zhuang, G., Zhang, H., Wu, H., Zhang, Z., and Liao, L. (2017a) Influence of the
652 surfactants' nature on the structure and rheology of organo-montmorillonite in
653 oil-based drilling fluids. *Applied Clay Science*, **135**, 244-252.
654 Zhuang, G., Zhang, Z., Gao, J., Zhang, X., and Liao, L. (2017b) Influences of
655 surfactants on the structures and properties of organo-palygorskite in oil-based
656 drilling fluids. *Microporous and Mesoporous Materials*, **244**, 37-46.
657 Zhuang, G., Zhang, Z., Guo, J., Liao, L., and Zhao, J. (2015) A new ball milling method
658 to produce organo-montmorillonite from anionic and nonionic surfactants.
659 *Applied Clay Science*, **104**, 18-26.
660 Zhuang, G., Zhang, Z., Jaber, M., Gao, J., and Peng, S. (2017c) Comparative study on

the structures and properties of organo-montmorillonite and organo-palygorskite in oil-based drilling fluids. *Journal of Industrial and Engineering Chemistry*, **56**, 248-257.

Zhuang, G., Zhang, Z., Sun, J., and Liao, L. (2016) The structure and rheology of organo-montmorillonite in oil-based system aged under different temperatures. *Applied Clay Science*, **124**, 21-30.

FIGURE CAPTIONS:

Figure 1. XRD pattern of Mnt with the JCPDS cards of montmorillonite, quartz, calcite, albite, and pyrite.

Figure 2. Structural diagrams of organic cations with optimized geometrical shapes and molecular sizes.

Figure 3. XRD patterns of OMnt samples.

Figure 4. TEM images of Mnt and OMnt samples.

Figure 5. TG and corresponding DTG curves of Mnt, organic surfactants, and OMnt samples.

Figure 6. XPS survey scans of Mnt and OMnt samples.

Figure 7. O 1s high-resolution XPS spectra of Mnt and OMnt samples.

Figure 8. Si 2p high-resolution XPS spectra of Mnt and OMnt samples.

Figure 9. Al 2p high-resolution XPS spectra of Mnt and OMnt samples.

Figure 10. C 1s high-resolution XPS spectra of surfactants and OMnt samples.

Figure 11. N 1s high-resolution XPS spectra of surfactants and OMnt samples.

683 Figure 12. Schematic diagram of the different arrangements of surfactants in the
684 interlayer space of OMnt.
685 Figure 13. Dynamic rheological curves of OMnt/oil fluids aged at 66°C, 150°C,
686 180°C, and 200°C.
687 Figure 14. XRD results for OMnt/oil gels aged at 66°C, 150°C, 180°C, and 200°C.
688 Tables:
689
690 Table 1. K-values of selected minerals.

Mineral	(*hkl*)	°2θ	*d* value (nm)	K-value
Corundum	(104)	35.16	0.2550	1.00
Montmorillonite	(020)	19.80	0.4880	0.50
Quartz	(101)	26.65	0.3343	4.32
Calcite	(104)	29.42	0.3034	2.80
Albite	(002)	27.92	0.3193	1.80
Pyrite	(200)	33.00	0.2712	2.06

691
692
693 Table 2. A summary of the components in the Mnt sample.

Component	Montmorillonite	Quartz	Calcite	Albite	Pyrite
Mass (%)	88%	7%	2%	2%	1%

694
695

696 Table 3. Summary of basal spacings derived from XRD and TEM.

Sample	d_{001} (XRD)/nm	d_{001} (TEM)/nm	Δd_{001}/nm
C18-Mnt-1.0	2.12	1.44–1.79	0.33–0.68
C18-Mnt-2.0	4.06	1.87	2.19
DC18-Mnt-0.5	3.51	2.42	1.09
DC18-Mnt-1.0	3.68	2.53	1.15

697 Note: $\Delta d_{001} = d_{001}$ (XRD) – d_{001} (TEM)

698

699 Table 4. Summary of ΔBE values.

Sample	Δ BE (eV)		
	O 1s	C 1s (C-N)	N 1s
C18-Mnt-1.0	− 1.2	0.5	0.3
C18-Mnt-2.0	− 1.0	0.4	0.3
DC18-Mnt-0.5	− 1.1	0.5	0.2
DC18-Mnt-1.0	− 1.2	0.3	0.1

700 Note: ΔBE (O 1s) = BE (O 1s, OMnt) – BE (O 1s, Mnt); ΔBE (C 1s) = BE (C 1s,
701 OMnt) – BE (C 1s, surfactant); and ΔBE (N 1s) = BE (N 1s, OMnt) – BE (N 1s,
702 surfactant).

703

704 Table 5. Rheological properties of OMnt/oil fluids aged at different temperatures.

Sample	AV (mPa·s)	PV (mPa·s)	YP (Pa)

	66°C	150°C	180°C	200°C	66°C	150°C	180°C	200°C	66°C	150°C	180°C	200°C
DG-Mnt	16.0	17.0	15.5	15.0	16.0	16.0	15.0	15.0	0.0	1.0	0.5	0.0
C18-Mnt-1.0/oil	14.5	15.0	15.0	14.0	14.5	14.5	14.5	14.0	0.0	0.5	0.5	0.0
C18-Mnt-2.0/oil	16.5	31.0	26.5	24.0	16.0	16.0	21.0	21.0	0.5	15.0	5.5	3.0
DC18-Mnt-0.5/oil	15.0	15.0	16.0	15.0	15.0	14.5	16.0	14.5	0.0	0.5	0.0	0.5
DC18-Mnt-1.0/oil	24.5	47.0	43.0	40.0	21.0	29.0	26.0	25.0	3.5	18.0	17.0	15.0

Table 6. Areas of thixotropic loops derived from Figure 13.

Sample	Areas of thixotropic loops ($Pa \cdot s^{-1}$)			
	66°C	150°C	180°C	200°C
DG-Mnt/oil	4.25	3.65	3.07	4.45
C18-Mnt-1.0/oil	1.62	1.64	1.52	1.45
C18-Mnt-2.0/oil	2.61	193.43	75.50	27.50
DC18-Mnt-0.5/oil	3.40	3.84	1.65	1.43
DC18-Mnt-1.0/oil	26.21	424.68	394.94	342.85

FIGURES:

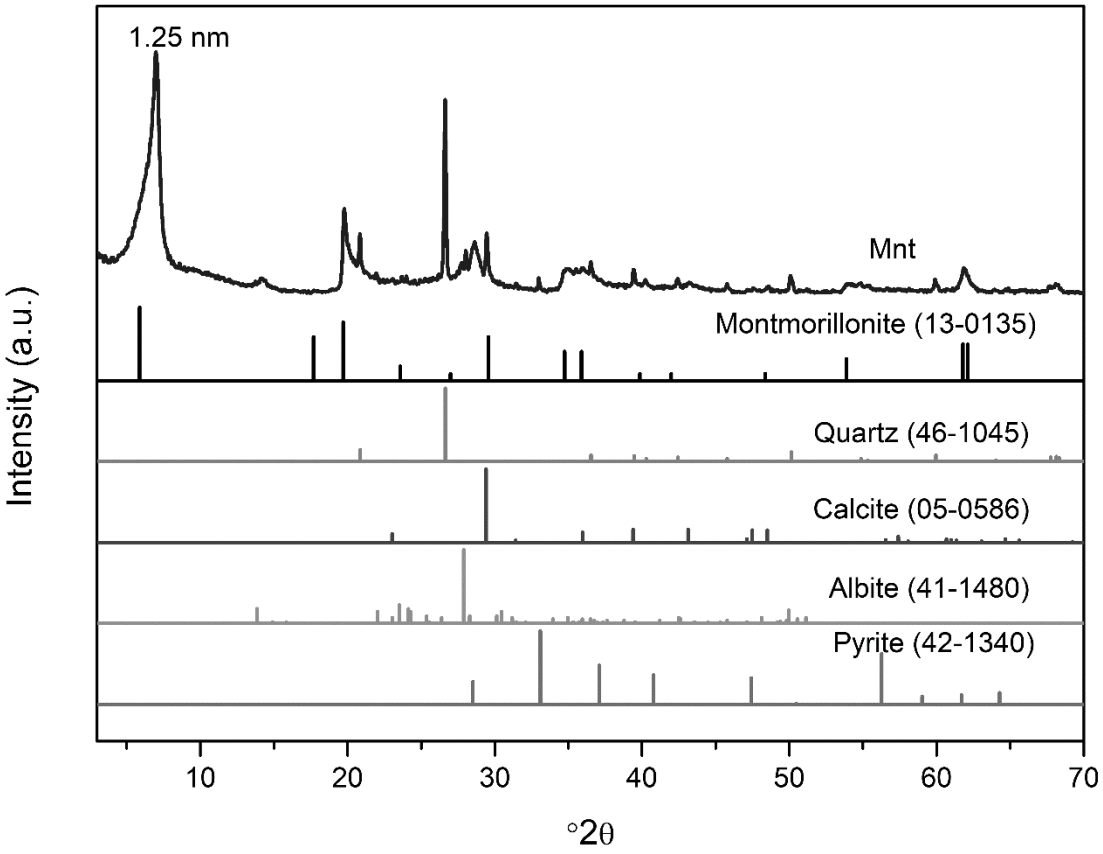

712

713 Figure 1 XRD pattern of Mnt with the JCPDS cards of montmorillonite, quartz,

714 calcite, albite and pyrite.

715

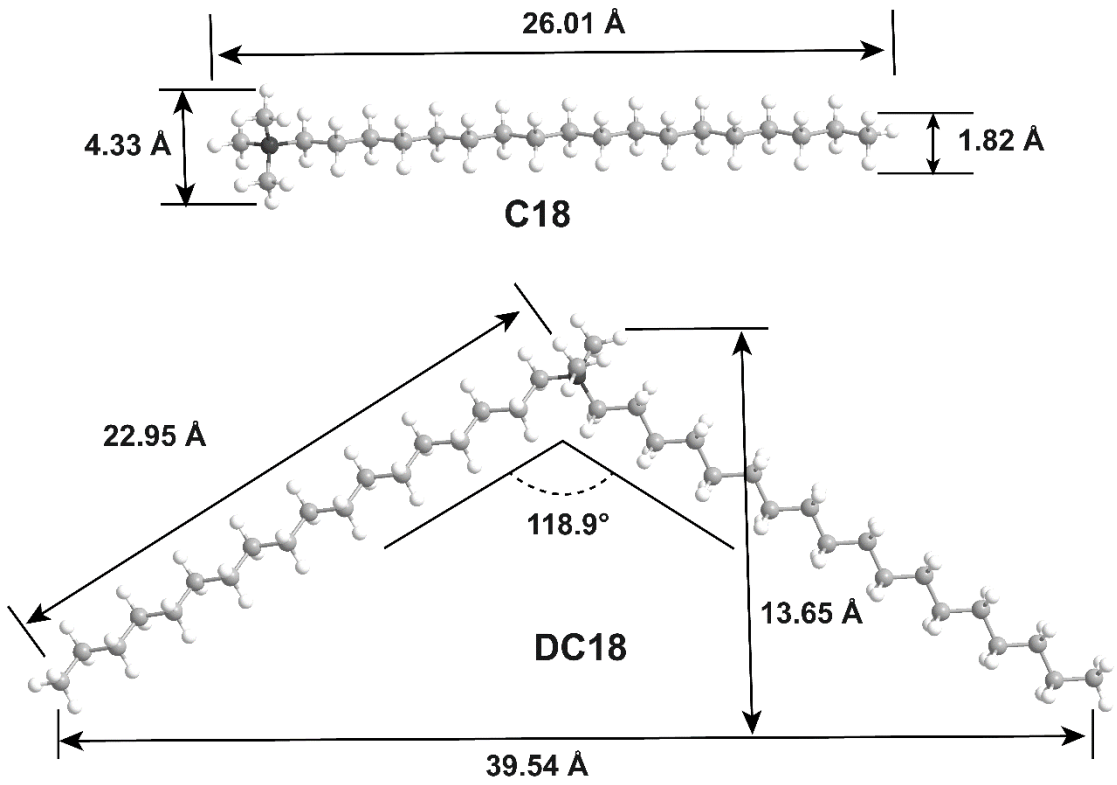

Figure 2 Structural diagrams of organic cations with the optimized geometrical shapes and molecular sizes.

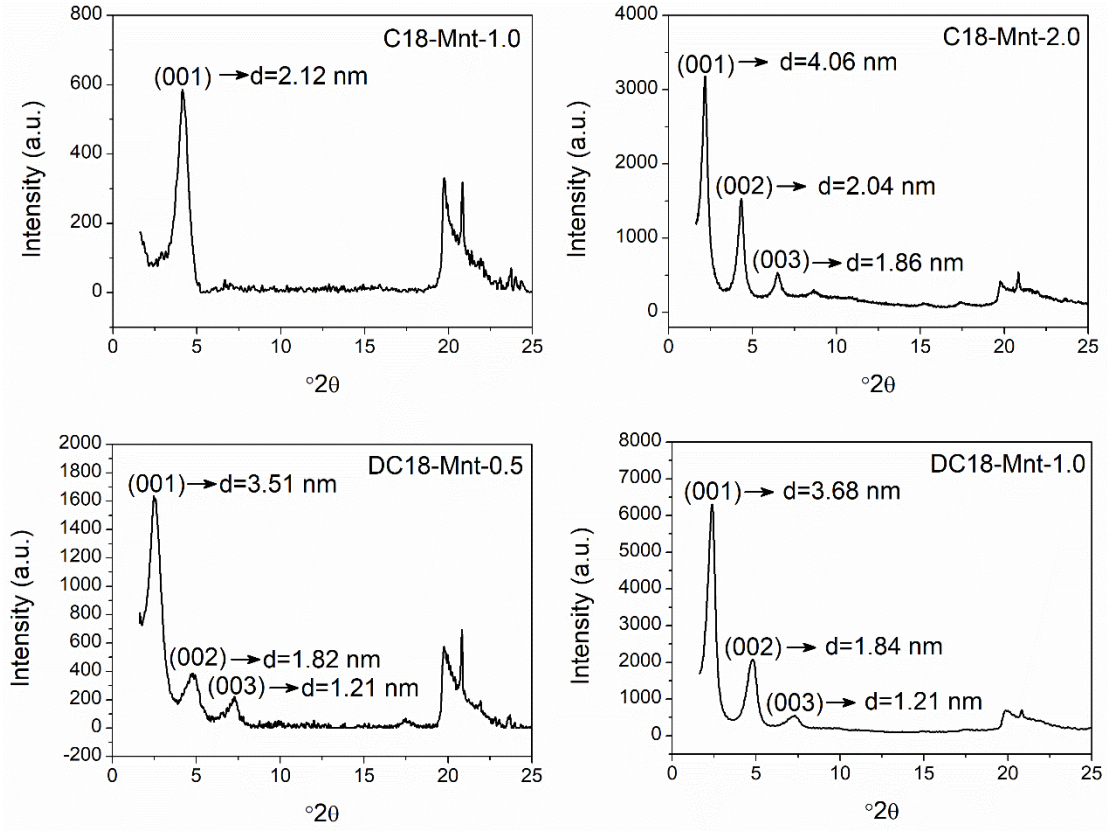

720

721 Figure 3 XRD patterns and OMnt samples.

722

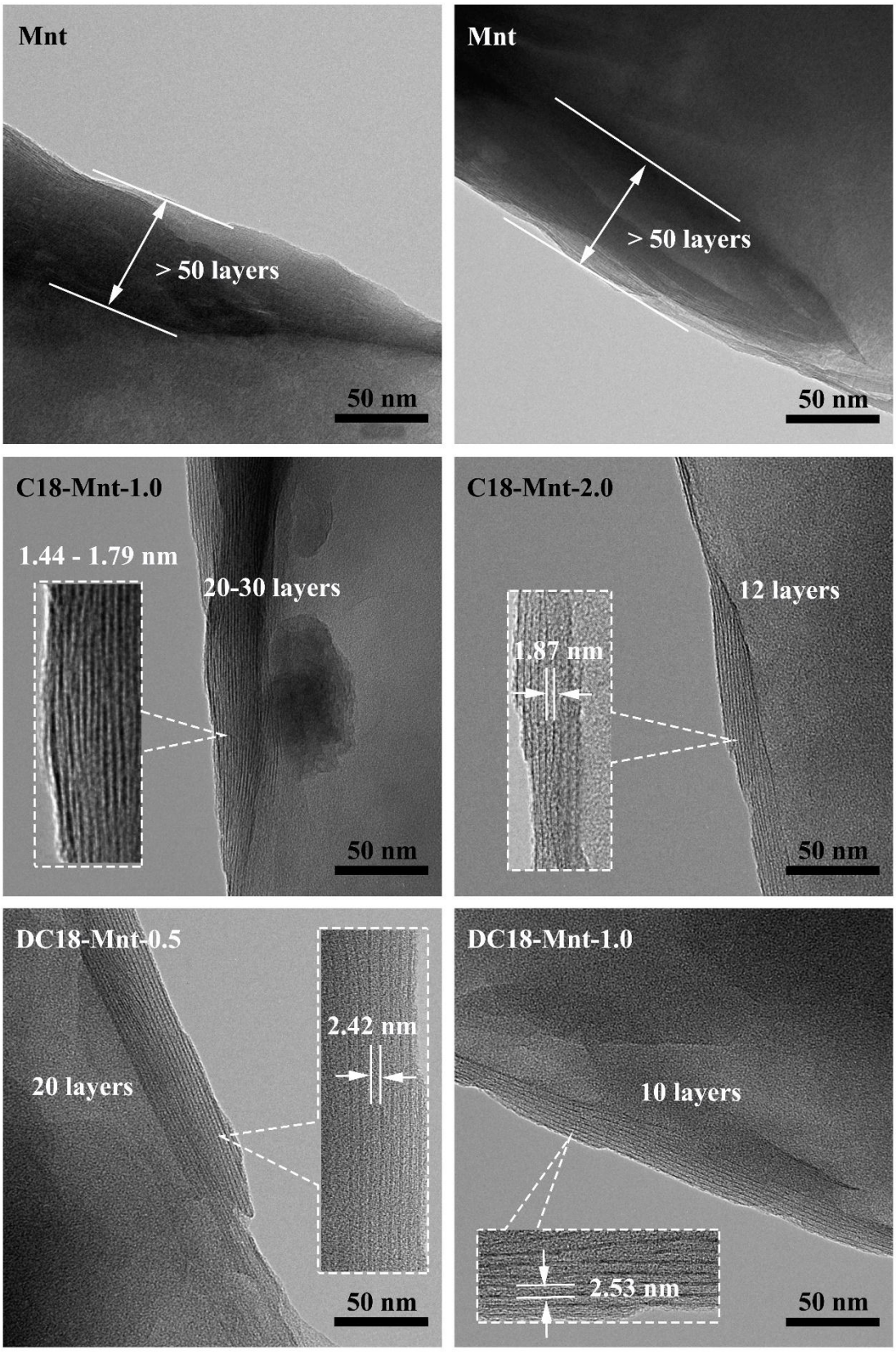

723

724 Figure 4 TEM images of Mnt and OMnt samples.

725

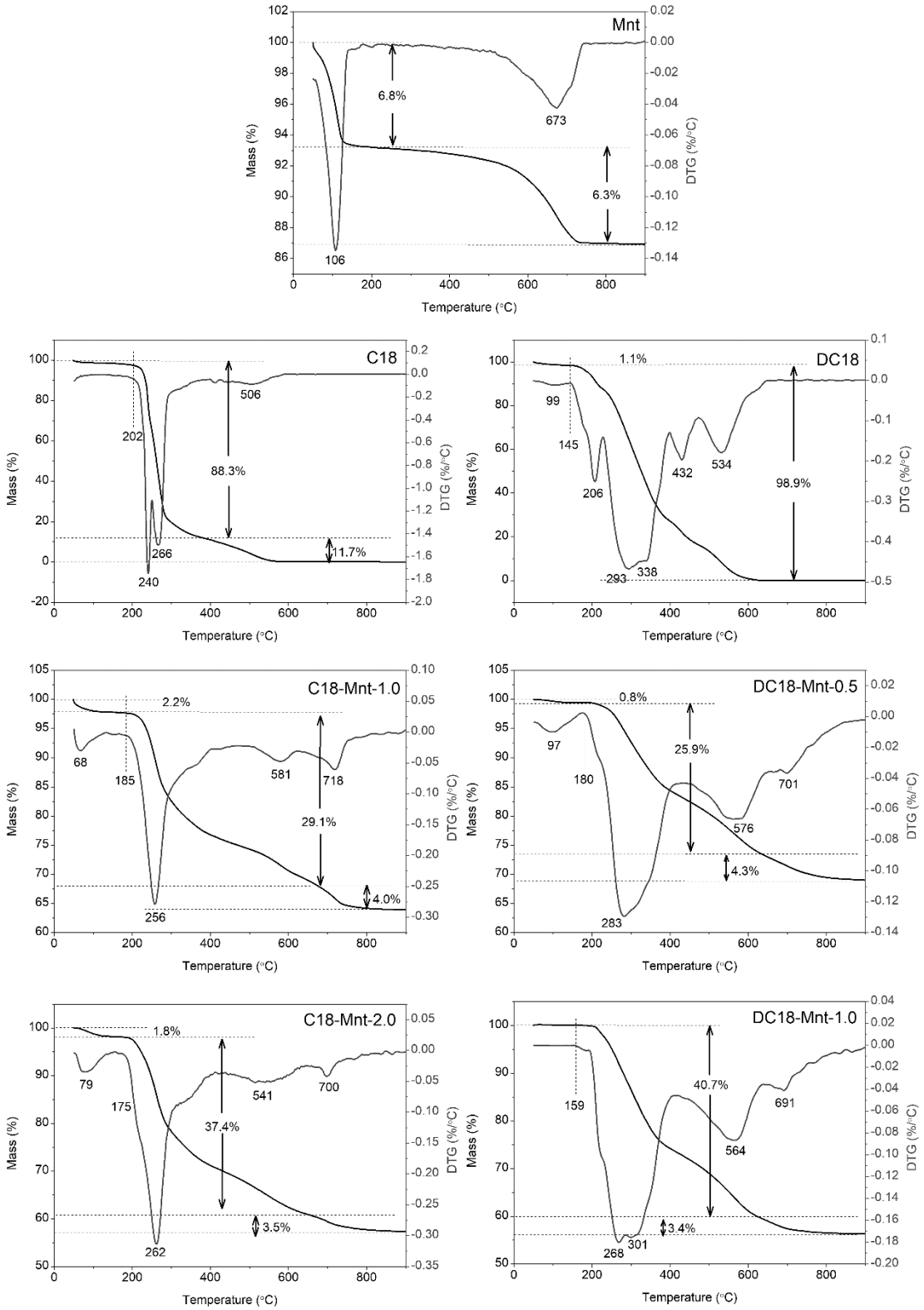

Figure 5 The TG and corresponding DTG curves of Mnt, organic surfactants, and OMnt samples.

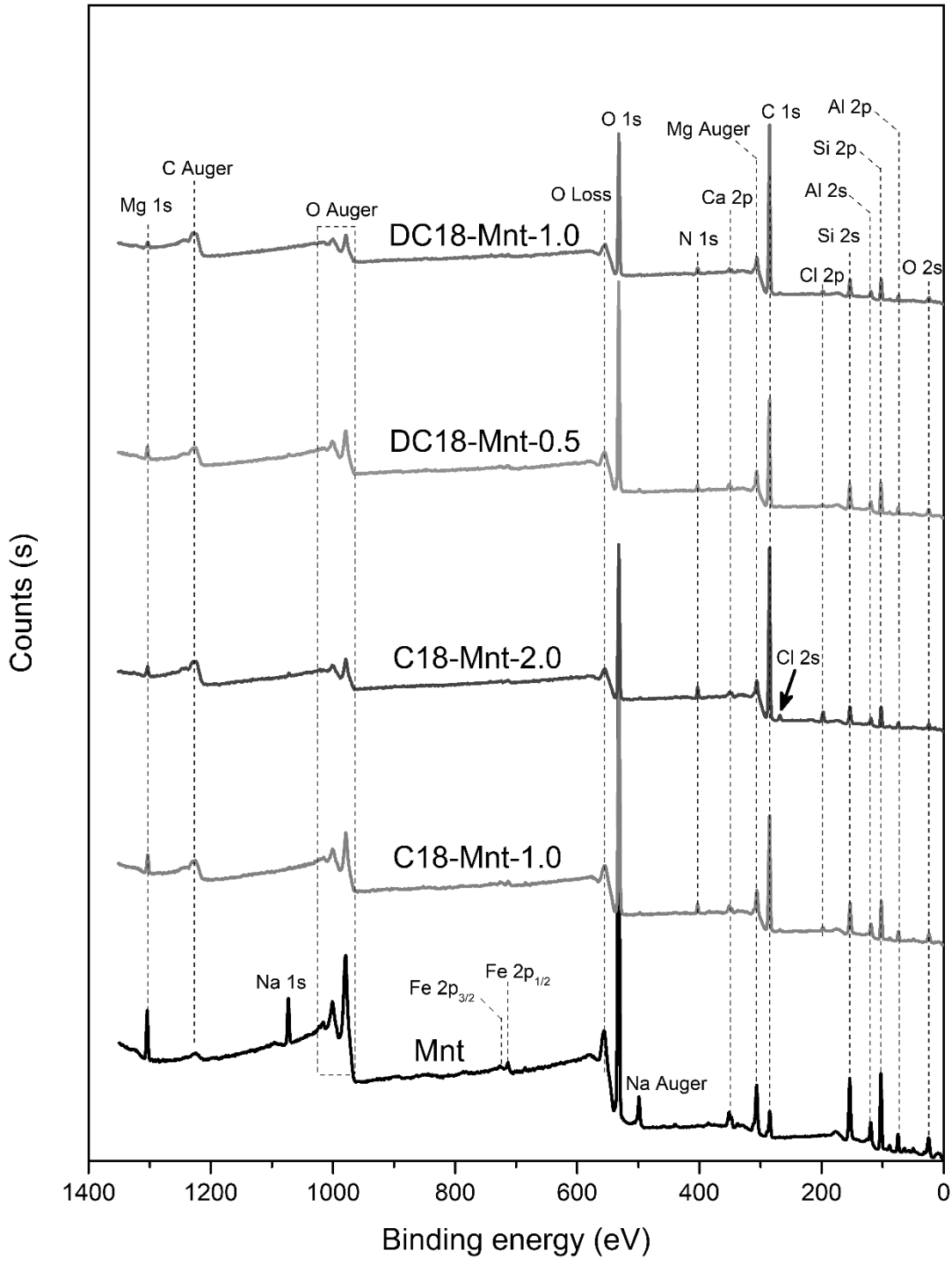

730

731 Figure 6 Survey scans of Mnt and OMnt samples.

732

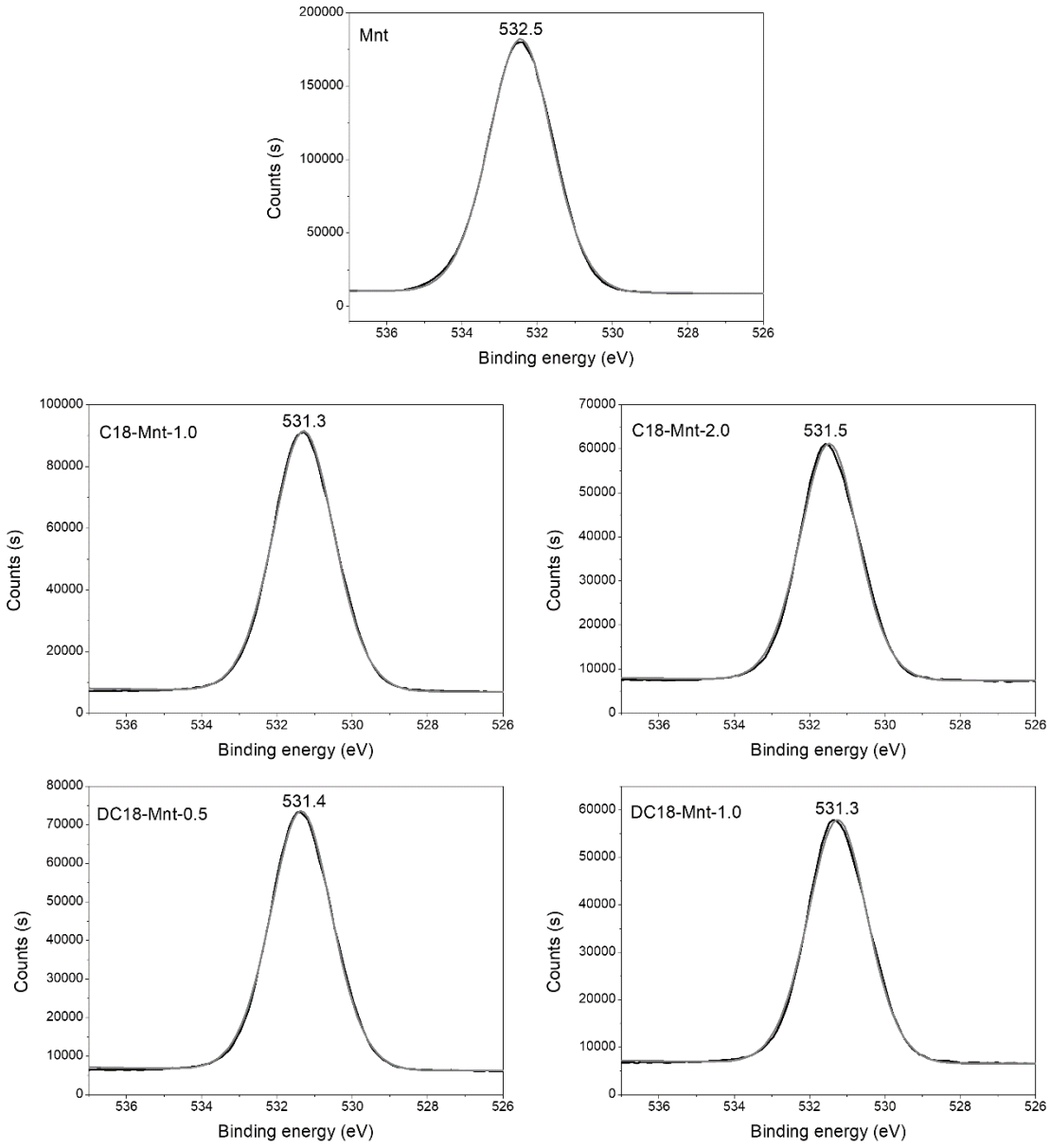

733

734 Figure 7 O 1s high-resolution XPS spectra of Mnt and OMnt samples.

735

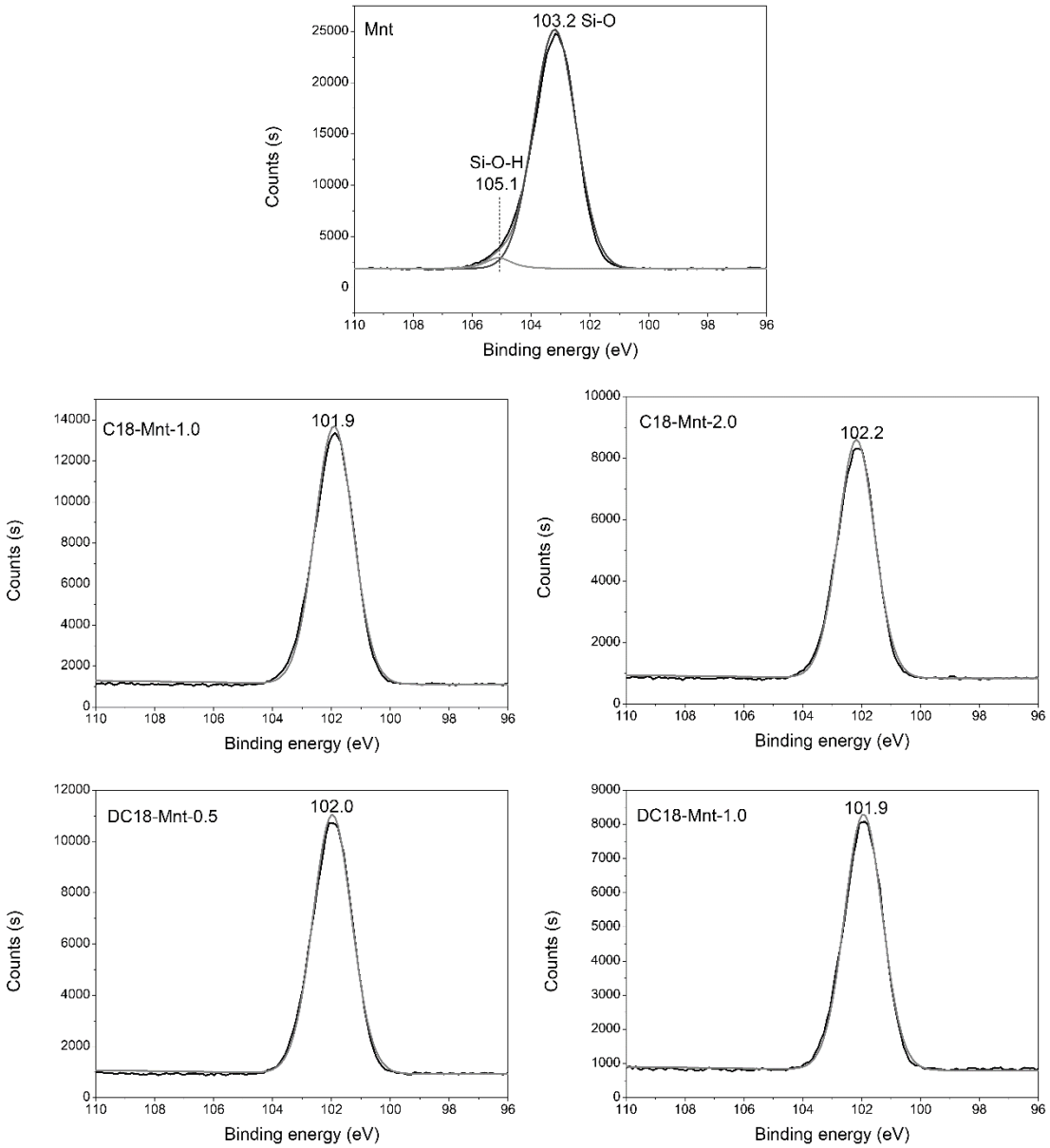

736

737 Fig. 8 Si 2p high-resolution XPS spectra of Mnt and OMnt samples.

738

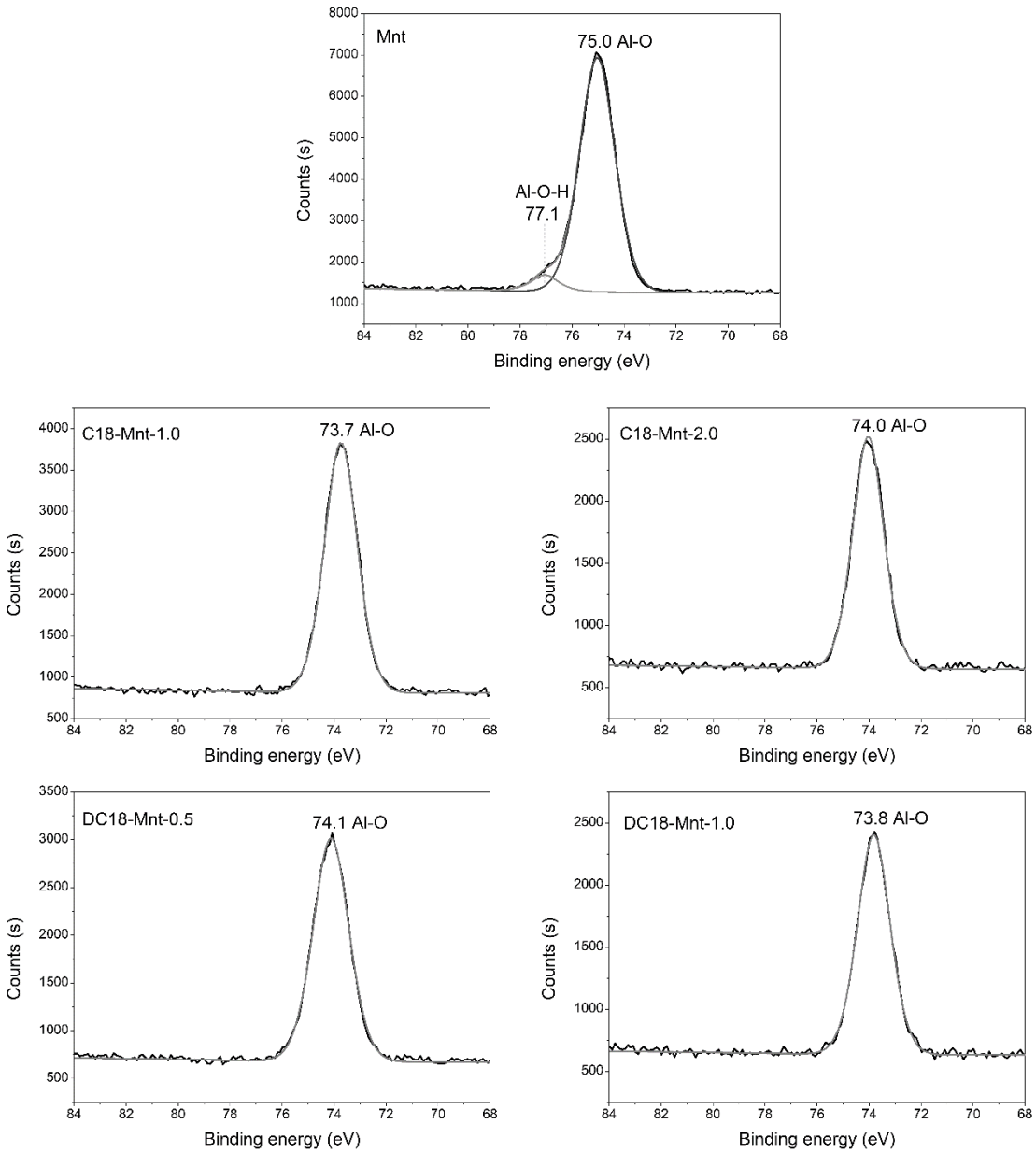

739

740 Fig. 9 Al 2p high-resolution XPS spectra of Mnt and OMnt samples.

741

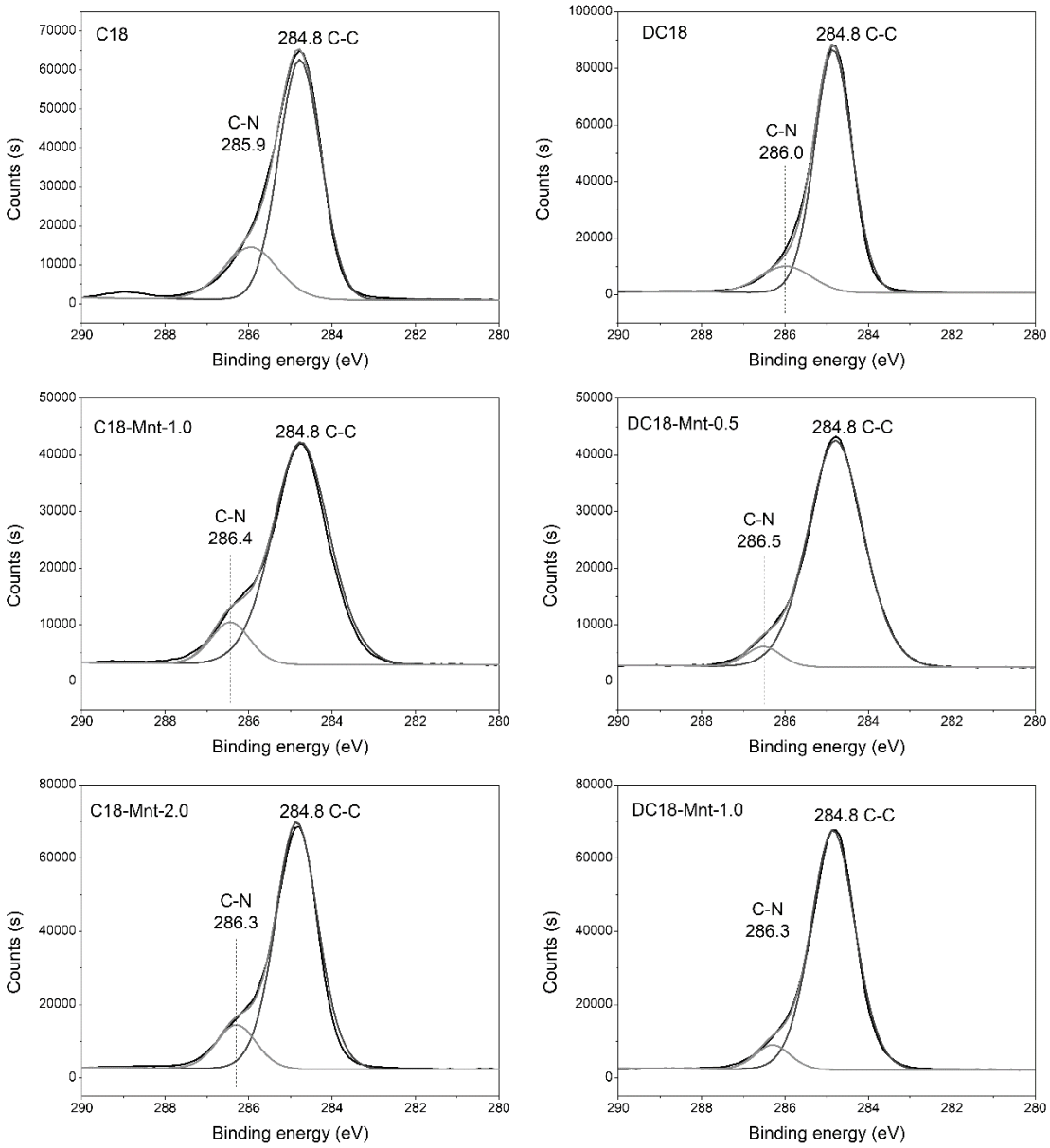

742

743 Figure 10 C 1s high-resolution XPS spectra of surfactants and OMnt samples.

744

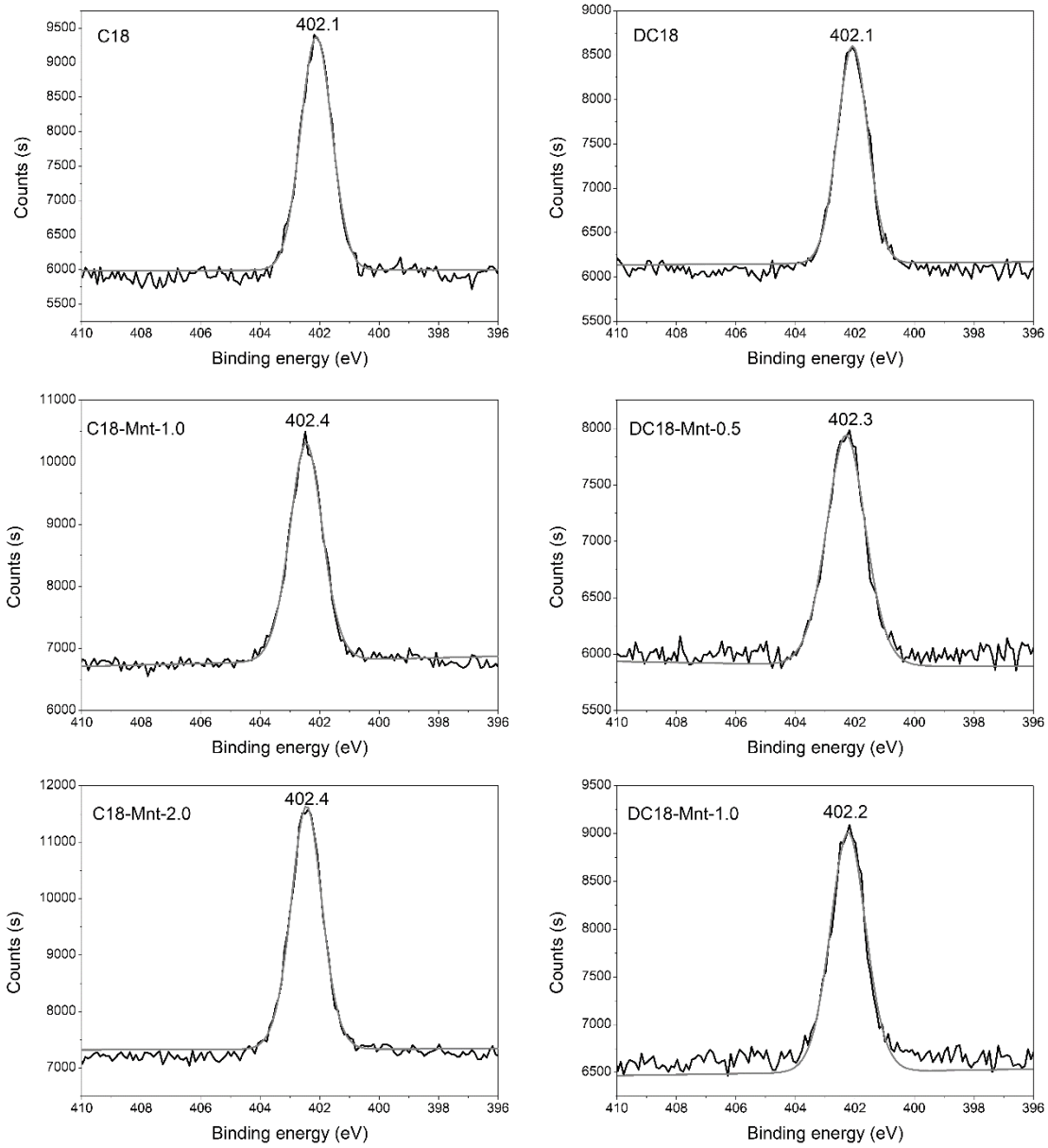

745

746 Figure 11 N 1s high-resolution XPS spectra of surfactants and OMnt samples.

747

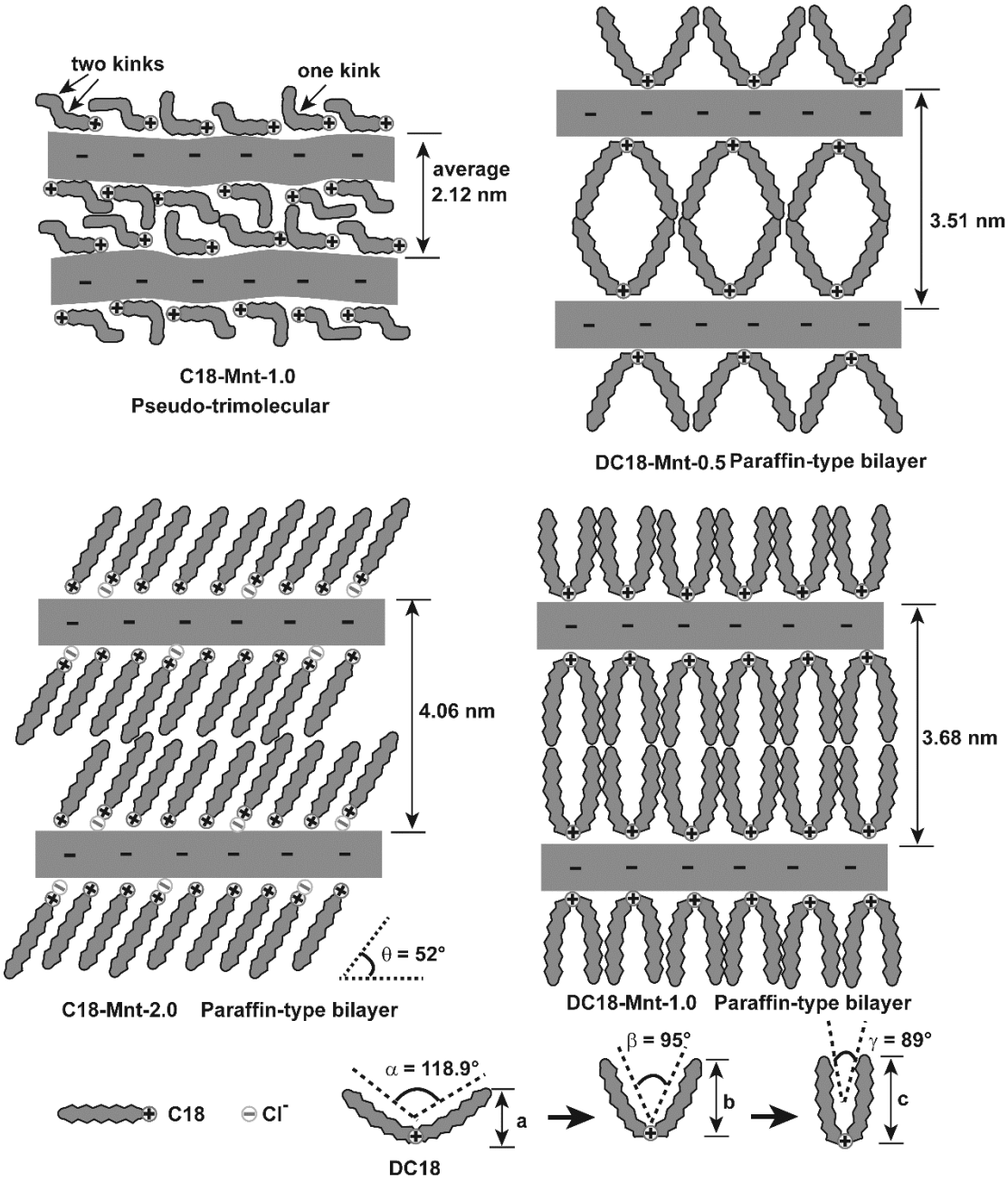

748

749 Figure 12 Schematically interpretive diagram of arrangements of surfactants in the

750 interlayer space of OMnt.

751

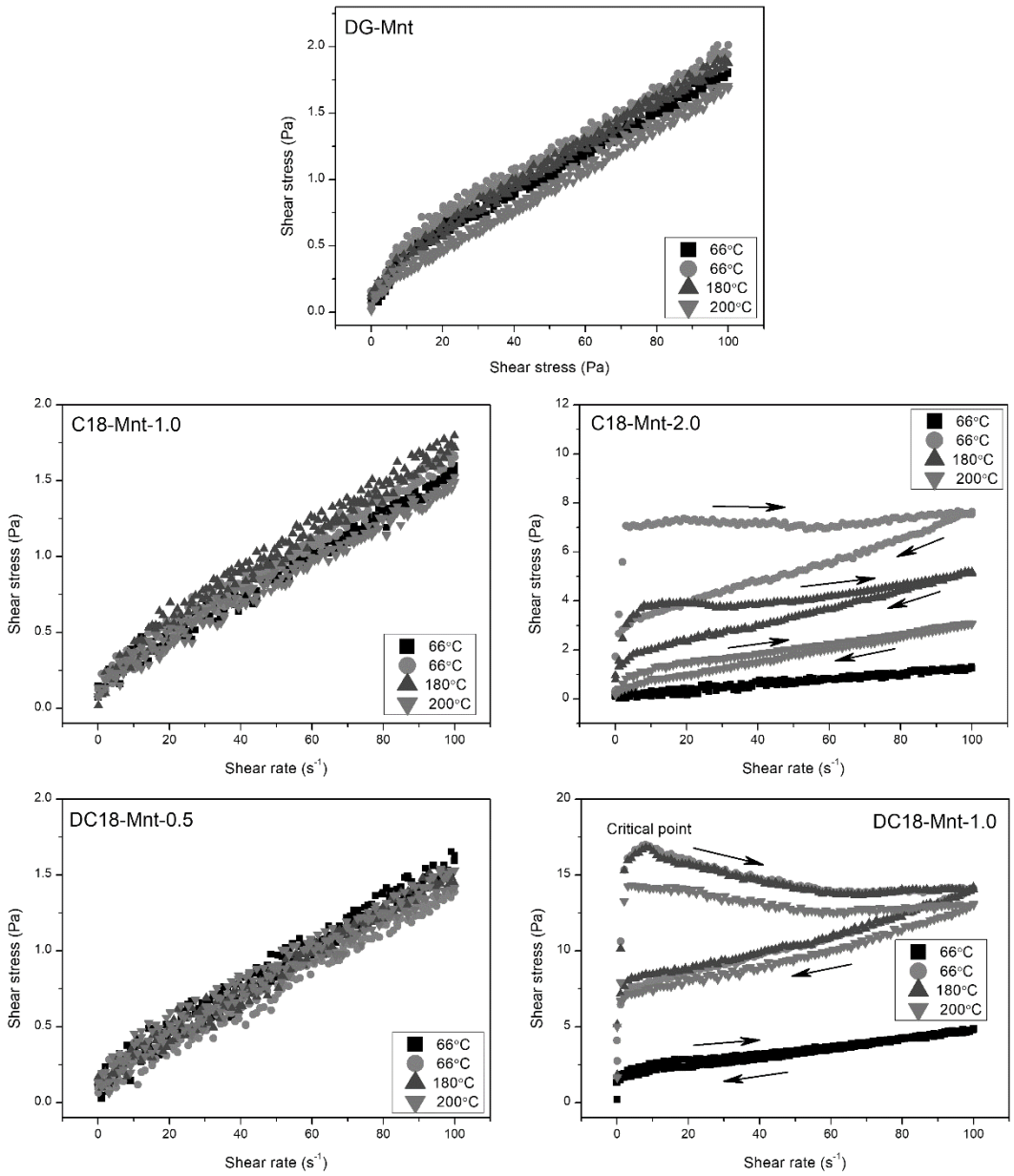

752

753 Figure 13 Dynamic rheological curves of OMnt/oil fluids aged at 66°C, 150°C, 180°C

754 and 200°C.

755

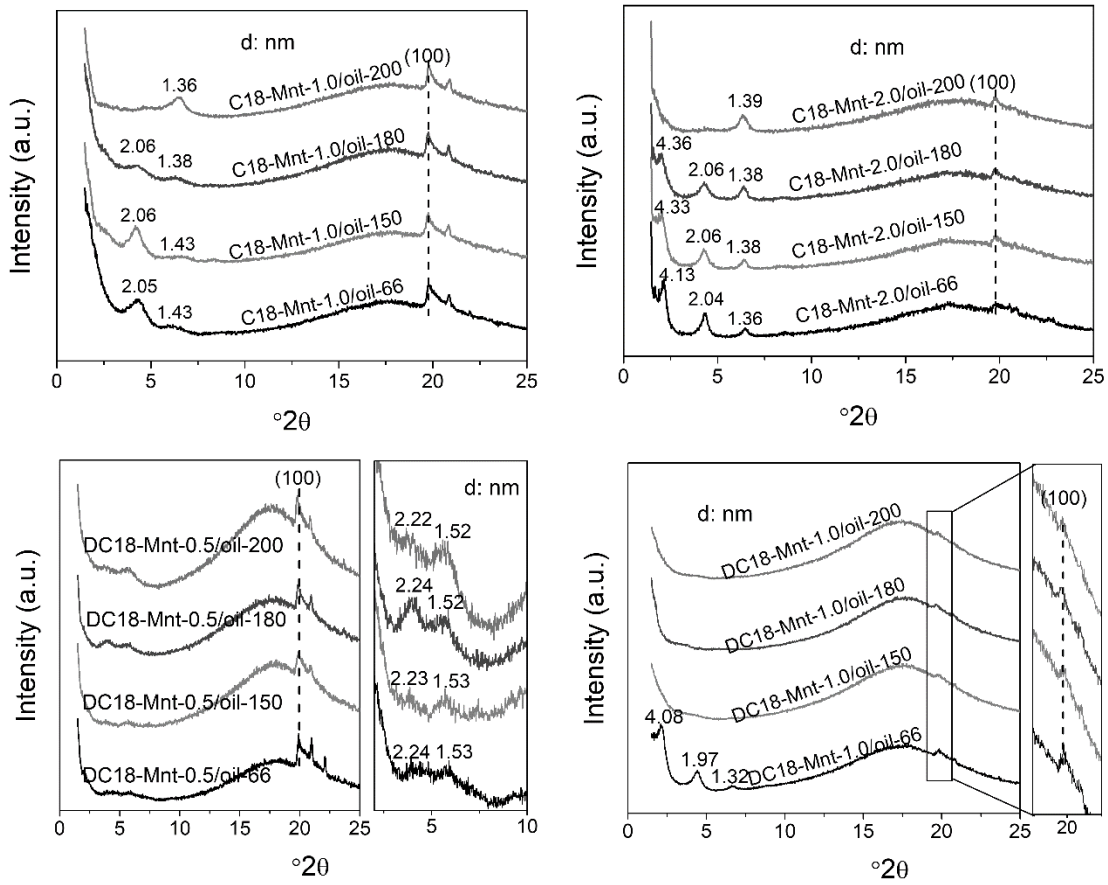

Figure 14 XRD results of OMnt/oil gels aged at 66°C, 150°C, 180°C and 200°C.